RSC Advances

PAPER

View Article Online
View Journal | View Issue

Cite this: *RSC Adv.*, 2017, **7**, 19912

The enhanced resistance to P species of an Mn–Ti catalyst for selective catalytic reduction of NO_x with NH_3 by the modification with Mo

Rui-tang Guo,*[ab] Ming-yuan Li,[ab] Peng Sun,[ab] Shu-ming Liu,[ab] Shu-xian Wang,[ab] Wei-guo Pan,*[ab] Shuai-wei Liu,[ab] Jian Liu[ab] and Xiao Sun[ab]

Received 15th February 2017
Accepted 29th March 2017

DOI: 10.1039/c7ra01876b

rsc.li/rsc-advances

Phosphorous has a deactivation effect on an SCR catalyst. In this study, the effect of Mo modification on the resistance to P species of a Mn–Ti catalyst for selective catalytic reduction of NO_x with NH_3 was investigated. It was found that the addition of Mo could greatly improve the P species tolerance of the Mn–Ti catalyst. From the characterization results of BET, XRD, H_2-TPR, NH_3-TPD and XPS, it could be concluded that the modification of the Mn–Ti catalyst by Mo could enhance its specific surface area, redox ability and NH_3 adsorption capacity, along with the generation of more surface chemisorbed oxygen species, as a result, greatly enhancing the P species resistance of the Mn–Ti catalyst. The results of an *in situ* DRIFT study indicated that the NH_3-SCR reactions over Mn–Ti and Mn–Mo–Ti catalysts were governed by L–H mechanism (≤200 °C) and E–R mechanism (>200 °C) respectively.

1. Introduction

Emission of NO_x due to the combustion of fossil fuels in stationary and mobile sources has brought about a great amount of environmental issues including acid rain, photochemical smog, haze formation and ozone depletion.[1–6] Selective catalytic reduction of NO_x with NH_3 is the state of the art for NO_x emission abatement from stationary sources such as coal-fired power plants and municipal solid waste (MSW) incinerators.[7–9] V-based catalysts (mainly V_2O_5–WO_3/TiO_2 and V_2O_5–MoO_3/TiO_2) are the prevailing catalysts used in this process, which exhibit high SCR activity in the temperature range of 300–400 °C.[10] However there are still some inevitable disadvantages associated with this type of catalyst in practical application, including the high conversion of SO_2 to SO_3, N_2O generation at high temperature and the toxicity of vanadia to the environment and humans.[11–14] Moreover, the deactivation of V-based catalyst by SO_2, alkali/alkali earth/heavy metals and phosphorus greatly weakens its SCR performance.[15–22] Therefore, much effort has been put into developing green catalyst with high efficiency for further application.

Due to the presence of various types of labile oxygen in manganese oxides, Mn-based catalyst exhibits excellent performance in low-temperature NH_3-SCR reaction.[23–26] Moreover, the environmental-friendly property of manganese oxides offers competitive advantage for the future application of Mn-based SCR catalyst. Recently, the NH_3-SCR reaction over Mn-based catalyst has been investigated intensively by many research groups.[27–38] The SCR reactor using Mn-based catalyst could be installed downstream of the electrostatic precipitator of power plants, where the concentrations of fly ash is greatly decreased. However, the deactivation of Mn-based SCR catalyst by the impurity components of flue gas is still a concern.[39–42] Lately, the modification of Mn/TiO_2 catalyst by some transitional metals such as Ce, Co and Nb has been proven to be an effective method to enhance the resistance of Mn-based catalyst to alkali and heavy metals.[43–45] It is well recognized that P is enriched in the fly ash of sewage sludge incinerators (SSI).[46] The study of Cyr *et al.*[47] reported that the concentration of P in the fly ash of SSI was about 5–10 wt%. And the poisoning effect of P on SCR catalyst has been investigated by many researchers.[48–50] However, enhancing the P resistance of SCR catalyst has not been reported in the literatures till now. In this study, Mn–Ti catalyst was modified by Mo to promote its P resistance in SCR reaction, and the mechanism would be discussed based on the characterization results.

2. Experimental

2.1 Catalyst preparation

The fresh Mn–Ti and Mn–Mo–Ti catalyst samples were prepared by using coprecipitation method. Manganese nitrate, ammonium molybdate (when used) and titanium sulfate were used as the sources of Mn, Mo and Ti respectively. A certain amount of manganese nitrate, ammonium molybdate (when used) and titanium sulfate were fully dissolved in deionized water, followed by the addition of ammonia solution (3 mol L^{-1})

[a]School of Energy Source and Mechanical Engineering, Shanghai University of Electric Power, Shanghai, P. R. China. E-mail: grta@zju.edu.cn; pweiguo@163.com
[b]Shanghai Engineering Research Center of Power Generation Environment Protection, Shanghai, P. R. China

dropwisely under aqueous stirring at room temperature to the solution until its pH value reached 11. Then the sediment was filtered and washed thoroughly with deionized water after aged for 3 h. After dried at 110 °C overnight, the sample was calcined at 500 °C in air for 5 h. The molar ratios of Mn/Ti in Mn–Ti catalyst and Mn/Mo/Ti in Mn–Mo–Ti catalyst were set as 0.25 : 1 and 0.2 : 0.05 : 1 respectively.

Next then, the P-poisoned catalyst samples were prepared by impregnation method. The fresh Mn–Ti and Mn–Mo–Ti catalyst samples were impregnated in aqueous H_3PO_4 solution with a certain concentration (the molar ratio of P/Mn or P/(Mn + Mo) was 2 : 5) under vigorous stirring at room temperature. Then the mixture was dried at 110 °C for 12 h, followed by calcination at 500 °C in air for 5 h. The two catalyst samples were denoted as Mn–Ti–P and Mn–Mo–Ti–P respectively.

2.2 Characterizations

Brunauer–Emmett–Teller (BET) surface areas were measured by N_2 adsorption at −196 °C on a Quantachrome Autosorb-iQ-AG instrument. The XRD patterns were recorded on a Bruker D8 Advance powder diffractometer with CuKα radiation. The data was collected over a 2θ range of 10–80° with a step size of 0.02°. To determinate the chemical states of the elements on catalyst surface, X-ray photoelectron spectroscopy (XPS) measurement was carried out on an ESCALAB250 (Thermo Scientific Corp., USA) with monochromatic AlKα radiation. The binding value of C 1s (284.6 eV) was chose as the standard for calibrating the binding energy shift due to surface charging effect.

Temperature programmed reduction of H_2 (H_2-TPR) and temperature programmed desorption of NH_3 (NH_3-TPD) were all performed on a Quantachrome Autosorb-iQ-C chemisorption analyzer using 50 mg catalyst samples. Prior to TPR experiments, the catalyst sample was pretreated in pure Ar at 500 °C for 1 h. Then TPR runs were performed with a linear heating rate of 10 °C min^{-1} in pure Ar containing 5% H_2 at a flow rate of 40 mL min^{-1}. For NH_3-TPD experiments, after pretreatment in He environment at 400 °C for 1 h, the catalyst sample was cooled down to room temperature, then it was saturated with anhydrous NH_3 (4% in He) at a flow rate of 30 mL min^{-1} for about 30 min. Desorption was carried out by heating the sample in He environment (30 mL min^{-1}) from 100 °C to 500 °C with a heating rate of 10 °C min^{-1}. The consumption of H_2 during TPR experiment and the amount of NH_3 desorption during TPR experiment were all measured by a thermal conductivity detector (TCD).

NO_x-TPD experiments were performed in a fixed-bed reactor (i.d. = 8 mm) using 0.1 g catalyst sample. At first, the sample was pretreated with pure Ar at 450 °C for 1 h, then it was cooled down to room temperature. Next then, the sample was exposed to 500 ppm NO + 5% O_2/Ar (300 mL min^{-1}) for 1 h to reach the saturated adsorption of NO_x on it, followed by Ar purging (300 mL min^{-1}) for 1 h. At last, NO_x-TPD experiments were carried by heating the sample in Ar flow (300 mL min^{-1}) at a heating rate of 10 °C min^{-1} from room temperature to 500 °C. The desorption of NO_x was recorded by a continuous flue gas analyzer (Thermo, Model 42i-HL).

The *in situ* DRIFT measurements were performed on a FTIR spectrometer (Thermo Nicolet iS 50) with an MCT detector. In the DRIFT cell connected with a gas flow system, the catalyst sample was pretreated in Ar at 400 °C for 2 h and then cooled down to 50 °C in Ar. During the cooling process, the background spectra at certain temperature were recorded and automatically subtracted from the sample spectrum. During the *in situ* DRIFT experiments, the following conditions were used: 600 ppm NH_3 or/and 600 ppm NO + 5%O_2, balance with N_2, and the total flow rate was 300 mL min^{-1}. The DRIFT spectra were recorded by accumulating 32 scans with a resolution of 4 cm^{-1}.

2.3 Activity test

The SCR activity tests were performed in a fixed-bed quartz flow reactor (i.d. = 8 mm) at atmospheric pressure. The components of the simulated flue gas were as follows: 600 ppm NO, 600 ppm NH_3, 5% O_2 and balance Ar, with the total flow rate of 1 L min^{-1}. In each experimental run, about 0.55 cm^3 catalyst sample (80–100 mesh) was loaded, thus the gas hourly space velocity (GHSV) was 108 000 h^{-1}. Concentrations of NO, NO_2, NH_3 and N_2O were monitored by a Nicolet iS 50 spectrometer equipped with a gas cell with 0.2 dm^3 volume. The data for steady-state activity calculation were recorded after about 1 h at each temperature. The NO_x conversion and N_2 selectivity could be calculated by:

$$NO_x \text{ conversion} = \frac{[NO_x]_{in} - [NO_x]_{out}}{[NO_x]_{in}} \times 100\% \quad (1)$$

$$N_2 \text{ selectivity} = \left(1 - \frac{2[N_2O]_{out}}{[NO_x]_{in} + [NH_3]_{in} - [NO_x]_{out} - [NH_3]_{out}}\right) \times 100\% \quad (2)$$

The oxidation of NO to NO_2 was also measured in the same fixed-bed reactor as mentioned above. The compositions of reactants were as follows: 600 ppm NO, 5% O_2 and balance Ar, with the total flow rate of 1 L min^{-1}. And the GHSV was also kept at 108 000 h^{-1}.

3. Results and discussion

3.1 SCR performance

The SCR activities of the four catalyst samples as a function of reaction temperature are presented in Fig. 1. As can be seen from Fig. 1(A), the addition of Mo on Mn–Ti catalyst could enhance its SCR performance, especially in the lower temperature (≤200 °C). For Mn–Ti catalyst, a sharp decrease of NO_x conversion over it could be observed after the addition of P. It is noticeable that the NO_x conversion over Mn–Ti–P is no more than 70% in the whole experimental temperature range. Compared with Mn–Ti–P, the deactivation of Mn–Mo–Ti–P is relatively weaker. Moreover, the deactivation effect for the two poisoned catalyst samples becomes weaker with increasing temperature. The N_2 selectivities over the four catalyst samples are shown in Fig. 1(B). It is obvious that the loading of P would lead to the decrease of N_2 selectivities over Mn–Ti and Mn–Mo–Ti.

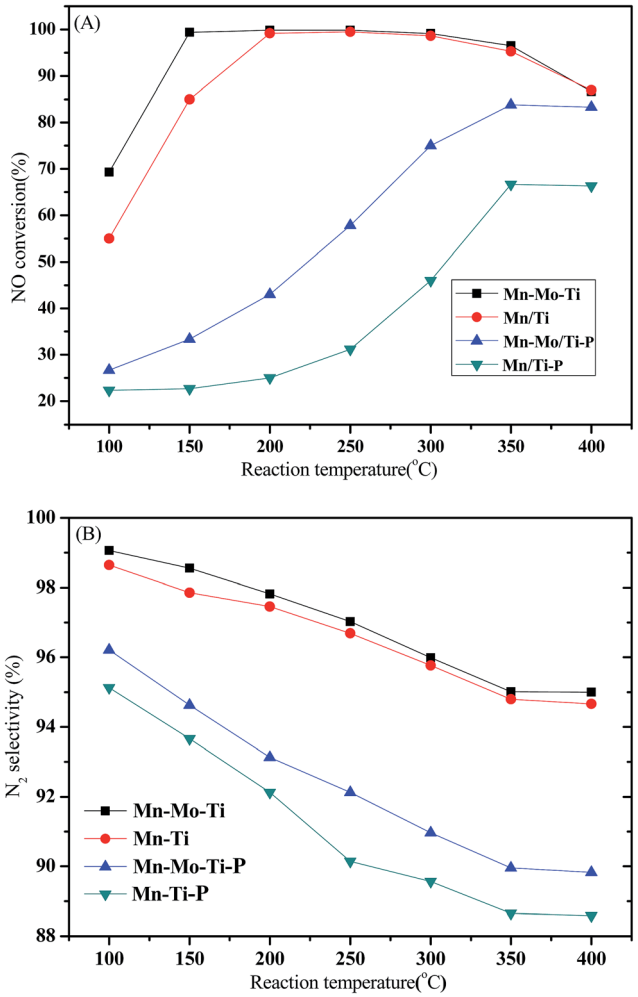

Fig. 1 (A) NO_x conversions and (B) N_2 selectivities over the four catalyst samples as a function of reaction temperature reaction conditions: [NO] = [NH_3] = 600 ppm, [O_2] = 5%, balance Ar, GHSV = 108 000 h^{-1}.

Table 1 BET measurements for the four catalyst samples

Samples	BET surface area (m^2 g^{-1})	Pore volume (cm^3 g^{-1})	Pore diameter (nm)
Mn–Ti	118.0	0.441	12.37
Mn–Mo–Ti	125.8	0.692	9.58
Mn–Ti–P	81.3	0.338	12.38
Mn–Mo–Ti–P	90.0	0.587	12.35

3.2 BET and XRD analysis

The BET surface areas of different catalyst samples are summarized in Table 1. It can be seen that Mn–Mo–Ti is of the largest BET surface and pore volume are among the four catalyst samples, which should be resulted from the strong interaction among Mn, Mo and Ti. After the addition of P, the BET surface areas of the two fresh catalyst samples decrease distinctly. The effect might be originated from the blocking effect of P species. Large BET surface are of Mn–Mo–Ti catalyst could enhance the adsorption of reactants on its surface, which is beneficial to the NH_3-SCR reaction over it.

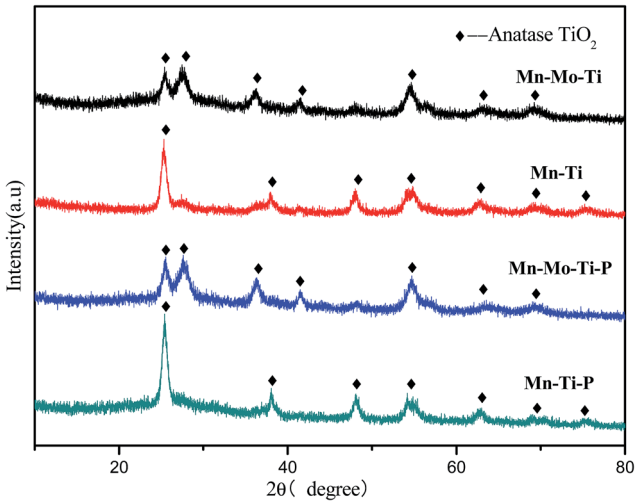

Fig. 2 XRD patterns of the four catalyst samples.

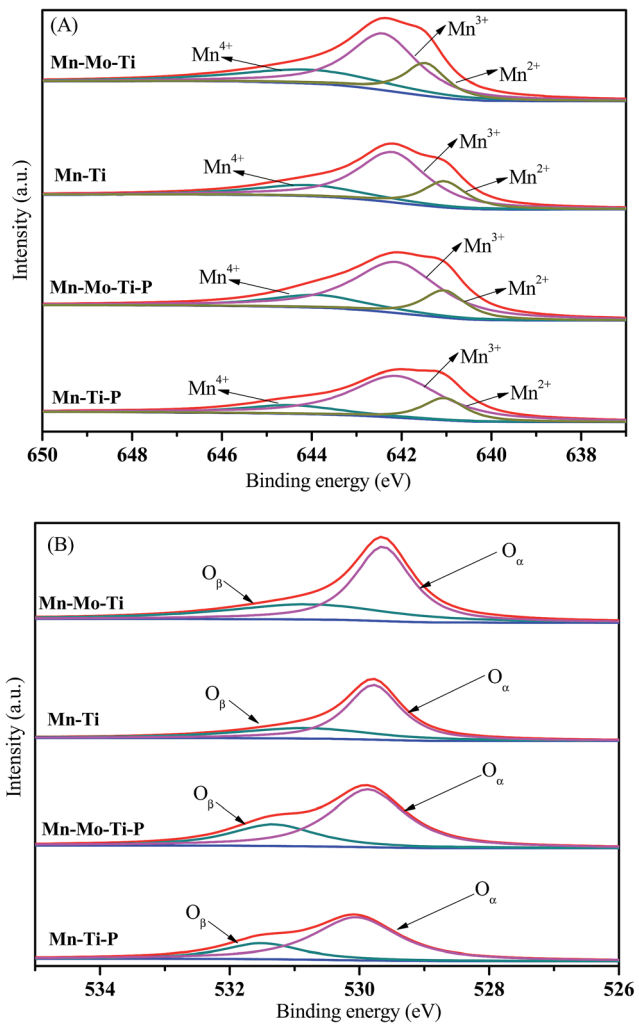

Fig. 3 (A) Mn $2p_{3/2}$ and (B) O 1s XPS spectra of the four samples.

The XRD patterns of different catalyst samples are illustrated in Fig. 2. From Fig. 2, only anatase phase TiO_2 could be detected in the XRD spectra of the four catalyst samples, indicating the

Table 2 Elemental surface analysis of the four catalyst samples (by XPS)

Samples	Mn (at%)	O (at%)	$Mn^{4+}/Mn^{2+} + Mn^{3+} + Mn^{4+}$ (%)	$O_\beta/(O_\alpha + O_\beta)$ (%)	P (at%)	Mn^{4+} (at%)	O_β (at%)
Mn–Ti	7.34	68.25	20.66	32.27	—	1.52	22.02
Mn–Mo–Ti	8.09	67.41	27.17	36.88	—	2.20	24.86
Mn–Ti–P	6.94	68.07	14.96	25.45	3.97	1.04	17.32
Mn–Mo–Ti–P	6.06	68.30	18.37	29.78	3.73	1.11	20.34

good dispersion of Mn, Mo and P species on catalyst surface. For the XRD spectra of the two fresh catalyst samples, it could be observed that the addition of Mo would decrease the peak intensities of anatase TiO_2. Thus the presence of Mo would result in lower crystallinity of Mn–Ti catalyst. Moreover several new diffraction peaks of anatase TiO_2 appeared after the addition of Mo, meanwhile, the diffraction peak of TiO_2 (1 0 1) in the shift to a higher 2θ value This feature indicates the incorporation of MoO_3 into TiO_2 lattice and the formation of solid solution.[51] On the contrary, the doping of P would promote the formation of anatase TiO_2 crystal, as indicated by the relatively higher diffraction peak intensities shown in the XRD spectra of Mn–Ti–P and Mn–Mo–Ti–P.

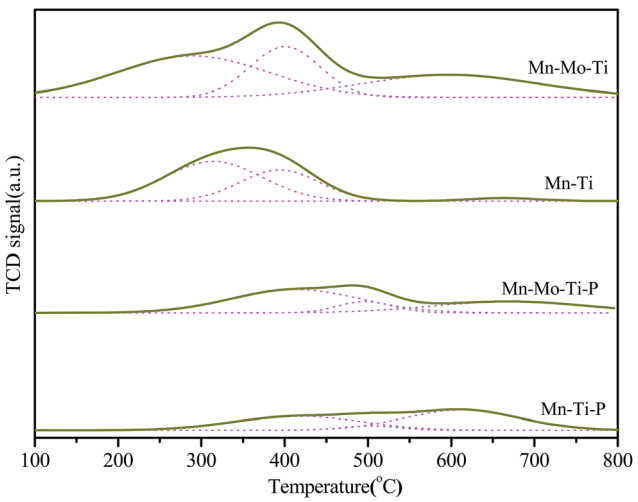

Fig. 4 H_2-TPR profiles of the four catalyst samples.

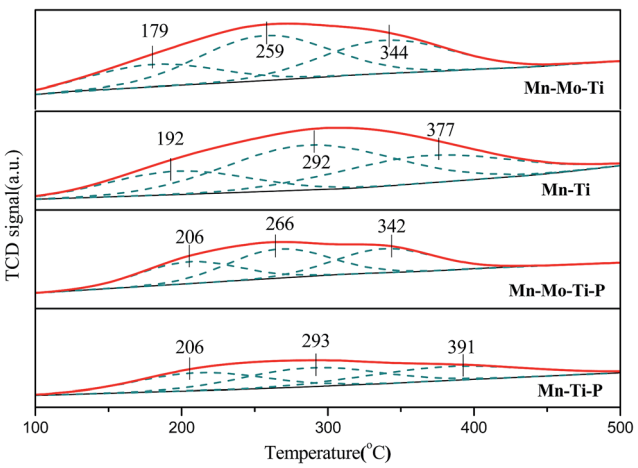

Fig. 5 NH_3-TPD profiles of the four catalyst samples.

3.3 XPS analysis

XPS analysis was performed to investigate the chemical states of elements on catalyst surface, and the results are shown in Fig. 3 and Table 2. As shown in Table 2, the surface concentrations of Mn species of the two fresh samples decrease after the loading of P, which might be resulted from the shielding/doping effect of P species on catalyst surface.

The Mn $2p_{3/2}$ XPS spectra of different catalyst samples could be observed in Fig. 3(A). According to previous studies,[52–54] the Mn $2p_{3/2}$ XPS spectra could be separated into three overlapped peaks belonging to Mn^{2+}, Mn^{3+} and Mn^{4+} respectively after a peak-fitting deconvolution. The surface atomic concentrations of Mn and O and the relative ratio of Mn^{4+} and chemisorbed

Table 3 Surface acidities of the four catalyst samples

Samples	Surface acidity (mmol g^{-1})
Mn–Ti	0.648
Mn–Mo–Ti	0.735
Mn–Ti–P	0.246
Mn–Mo–Ti–P	0.326

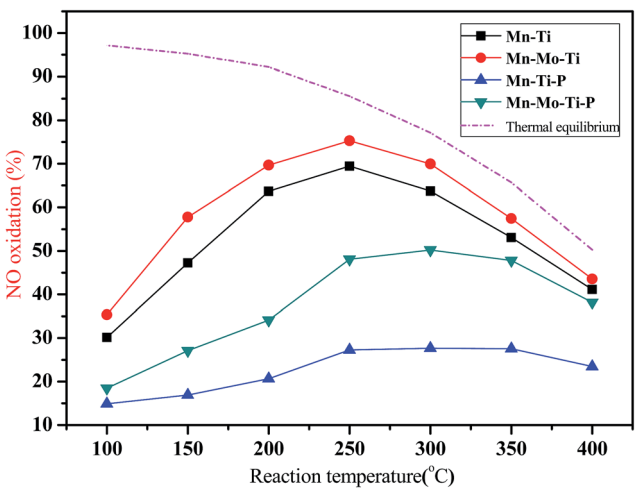

Fig. 6 NO oxidation over the four catalyst samples as a function of reaction temperature reaction conditions: [NO] = 600 ppm, $[O_2]$ = 5%, balance Ar, GHSV = 108 000 h^{-1}.

oxygen are all listed in Table 2. As can be seen from Table 2, the Mn^{4+} concentration over Mn–Mo–Ti catalyst is much higher than that over Mn–Ti catalyst, suggesting the generation of more Mn^{4+} over the surface of Mn–Ti catalyst by the modification with Mo. Based on previous studies,[7,55,56] the presence of more Mn^{4+} species could promote the oxidation of NO to NO_2, as a result, facilitating the "fast SCR" reaction and enhancing the low-temperature SCR activity.[57–59] Thus the low-temperature SCR activity of Mn–Mo–Ti catalyst is higher than that of Mn–Ti catalyst (Fig. 1(A)). Furthermore, the surface concentrations of Mn^{4+} of the two fresh catalyst samples decrease sharply after the addition of P. For instance, the surface concentration of Mn^{4+} of Mn–Mo–Ti catalyst is 2.20 at%, while the corresponding concentration of Mn–Mo–Ti–P is only 1.11 at%. As a result, the low-temperature SCR reactions over the two poisoned catalyst samples are greatly weakened, leading to their bad SCR performances at low temperature range.

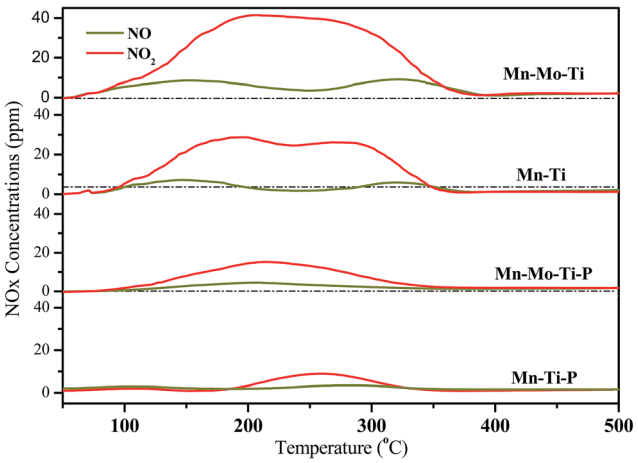

Fig. 7 NO_x-TPD profiles of the four catalyst samples.

The O 1s XPS spectra of different catalyst samples are exhibited in Fig. 3(B), which could be fitted into two peaks: lattice oxygen species O_α (529.0–530.0 eV) and chemisorbed oxygen species O_β (B. E. = 531.3–532.0 eV, mainly O_2^{2-} or O^- belonging to defect-oxide or hydroxyl-like group).[60,61] From Table 2, it is evident that the concentration of O_β over Mn–Mo–Ti catalyst (24.86%) is higher than that over Mn–Ti catalyst (22.02%). Due to its high mobility, the chemisorbed oxygen species are more active than lattice oxygen, which is beneficial to the oxidation of NO to NO_2 and the subsequent "fast SCR" reaction. Besides that, the presence of large amount surface hydroxyl-like groups could act as Brønsted acid sites to adsorb NH_3 and form NH_4^+. Next then, the generated NH_4^+ could react with NO_2 to form N_2 and H_2O.[62,63]

3.4 H_2-TPR analysis

H_2-TPR analysis was performed to investigate the reduction behavior of the four catalyst samples, and the results are exhibited in Fig. 4. From Fig. 4, it could be seen that there are three reduction peaks in the profile of each catalyst sample. For the

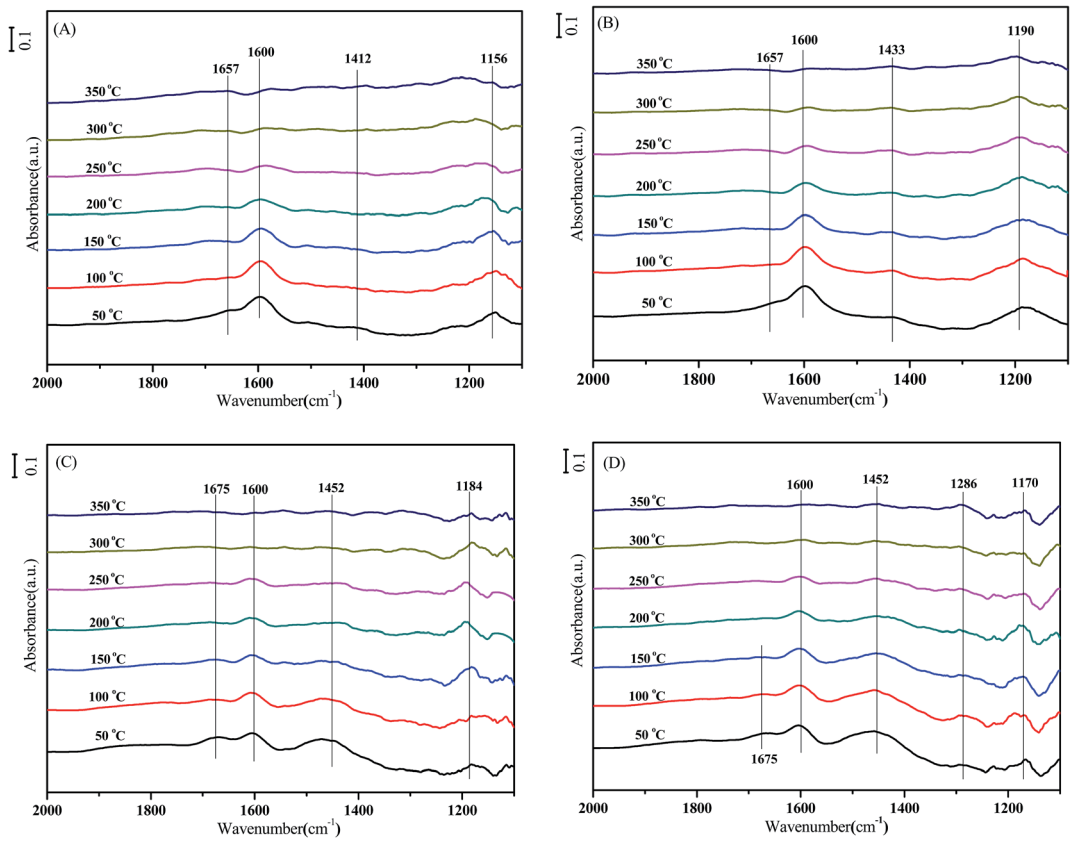

Fig. 8 *In situ* DRIFT spectra of NH_3 adsorption over (A) Mn–Ti; (B) Mn–Mo–Ti; (C) Mn–Ti–P and (D) Mn–Mo–Ti–P at different temperature.

profile of Mn–Ti catalyst, the first peak at about 310 °C could be assigned to the reduction of MnO_2/Mn_2O_3 to Mn_3O_4, the second peak at about 395 °C may be attributed to the reduction of Mn_3O_4 to MnO, and the third one at about 660 °C could be related to the reduction of the oxygen groups.[64–66] Thus the results of TPR analysis agree well with that of XPS analysis. It is noticeable that the reduction peaks in the profile of Mn–Ti catalyst move to lower value after the addition of Mo, as can be seen from the profile of Mn–Mo–Ti–P catalyst. Moreover, the reduction peak area of Mn–Mo–Ti catalyst is much larger than that of Mn–Ti catalyst, indicating the higher oxygen storage ability of Mn–Mo/TiO_2 catalyst. Thus the modification of Mn–Ti catalyst by Mo could greatly enhance its reducibility, which is helpful to complete the catalytic cycle in NH_3-SCR reaction and enhance the SCR performance. On the other hand, the loading of P would lead to the reduction peaks moving to higher temperature, accompanied by the great decrease of reduction peak area. Therefore, the addition of P on Mn–Ti or Mn–Mo–Ti catalyst would make the Mn species more stable and less reducible. Correspondingly, Mn–Ti–P and Mn–Mo–Ti–P only present bad low-temperature SCR performance, especially in the lower temperature range.

3.5 NH_3-TPD analysis

The adsorption of NH_3 species is a key step for NH_3-SCR reaction,[67,68] which is greatly dependent on the surface acidity of SCR catalyst. So the surface acidities of the four catalyst samples were determined by NH_3-TPD analysis, and the results are presented in Fig. 5. After a peak-fitting deconvolution, each profile could be separated into three peaks. The first one and the second one could be assigned to weak adsorption of ammonia on the catalyst samples, and the third one is NH_3 species strongly adsorbed on the catalyst.[69] From the peak area of each profile, the surface acidity of each catalyst sample could be obtained, as listed in Table 3. Apparently, the surface acidity of Mn–Ti catalyst increases by 13.4% after the addition of Mo. Thus the doping of Mo on Mn–Ti catalyst could promote the adsorption of NH_3 species on it. As a contrast, both the number and strength of the acid sites of the two fresh catalyst samples drop sharply after the introduction of P, which could be reflected by the low NH_3 adsorption capacities of them, as shown in Fig. 5 and Table 3.

3.6 NO oxidation

The oxidation of NO to NO_2 has a distinct promotion effect to NH_3-SCR reaction through "fast SCR" pathway: $NO + NO_2 + 2NH_3 \rightarrow 2N_2 + 3H_2O$.[70–72] Thus the NO catalytic activities over the four catalyst samples are tested and the results are illustrated in Fig. 6. From Fig. 6, it can be seen that the NO conversion curves exhibit a convex-parabola trend, indicating the conversion from kinetics-control to thermodynamics-control.[73] As presented in Fig. 6, the

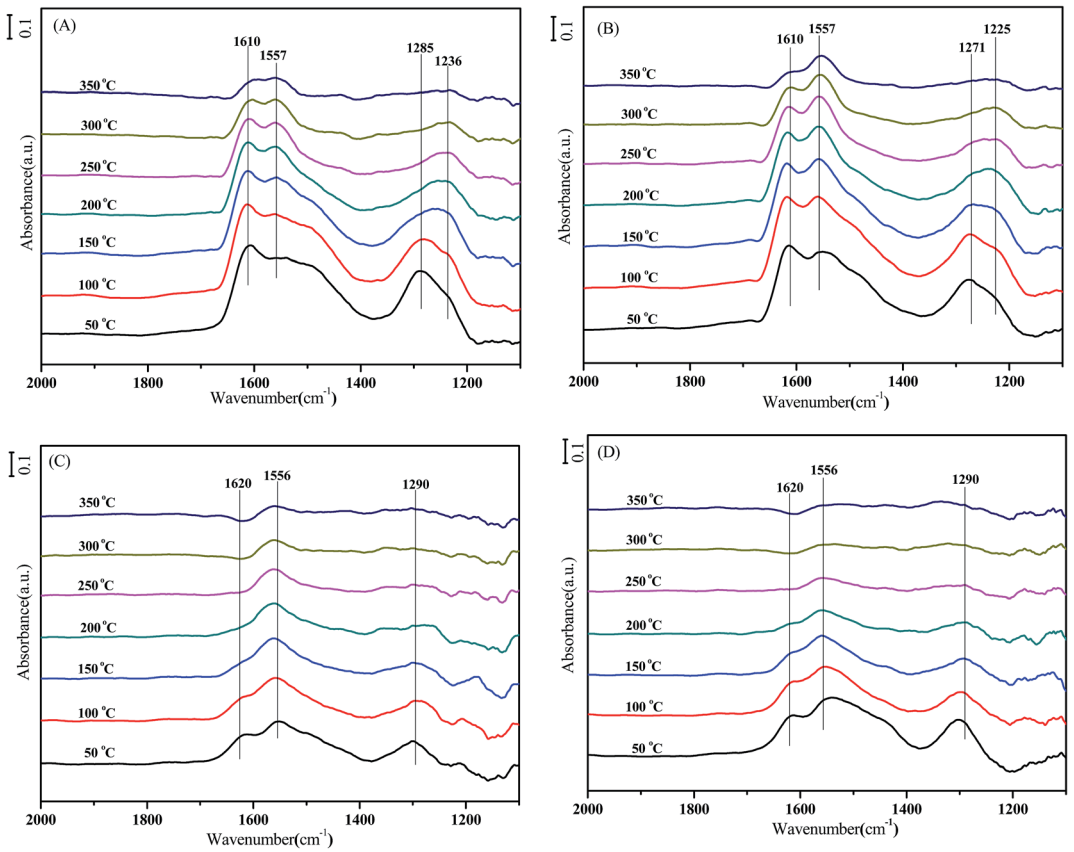

Fig. 9 *In situ* DRIFT spectra of NO + O_2 co-adsorption over (A) Mn–Ti; (B) Mn–Mo–Ti; (C) Mn–Ti–P and (D) Mn–Mo–Ti–P at different temperature.

addition of Mo on Mn–Ti catalyst could enhance the NO catalytic oxidation activity over it, as a result, facilitating the low-temperature SCR reaction. On the contrary, the loading of P would lead to the drop of activity for NO oxidation, correspondingly, inhibiting the low-temperature SCR reaction over the two poisoned catalyst samples. Therefore, the promoted NO oxidation over Mn–Ti catalyst after the addition of Mo could enhance its P resistance in low-temperature NH_3-SCR reaction.

3.7 NO_x-TPD analysis

NO_x-TPD analysis was performed to investigate the adsorption behavior of NO_x over the four catalyst samples, and the results are shown in Fig. 7. For Mn–Ti catalyst, two overlapped NO_2 desorption peaks could be found in the temperature range of 100–350 °C. For Mn–Mo–Ti catalyst, a broad NO_2 desorption peak lasting from 80–350 °C could be observed, and the peak area is a little larger than that of the NO_2 desorption peaks in the profile of Mn–Ti catalyst. Thus the modification of Mn–Ti catalyst with Mo could promote the oxidation of NO. For the two poisoned catalyst samples, only a weak NO_2 desorption peak could be detected in the profile of each catalyst. Moreover, two NO desorption peaks located at about 155 and 324 °C could be observed in the profiles of the two fresh catalyst sample, which could be ascribed to NO_x^-.[74] After the loading of P, only a very weak NO desorption peak appears in the profile of each poisoned catalyst sample. Therefore, the addition of P has a strong inhibition effect on both NO oxidation and adsorption, similar effect has also been reported in our recent study.[75]

3.8 *In situ* DRIFT study

In situ DRIFT study was performed to identify the active sites, adsorbed species and intermediates on catalyst surface in the NH_3-SCR process, thereby providing the evidence for mechanism analysis.

3.8.1 NH_3 adsorption. The *in situ* DRIFT spectra of NH_3 adsorption over Mn–Ti and Mn–Mo–Ti at different temperature are shown in Fig. 8. Several bands could be detected in the DRIFT spectra of the two catalyst samples, including species on Brønsted acid sites (1657, 1433 and 1412 cm^{-1}) and NH_3 species coordinated to Lewis acid sites (1600, 1190 and 1156 cm^{-1}).[76–80] Obviously, NH_3 species are mainly absorbed on Lewis acid sites, as reflected by the higher intensities of the corresponding bands. It is obvious that the band intensities of Lewis acid sites in the spectra of Mn–Mo–Ti catalyst are higher than that in the spectra of Mn–Ti catalyst, suggesting the presence of more Lewis acid sites for NH_3 adsorption on the surface of Mn–Mo–Ti catalyst. Thus the results of DRIFT study agree well with that of NH_3-TPD analysis. According to the results of XPS analysis, the surface concentration of Mn^{4+} over Mn–Mo–Ti is much higher than that over Mn–Ti catalyst. And the study of Meng *et al.*[81] has

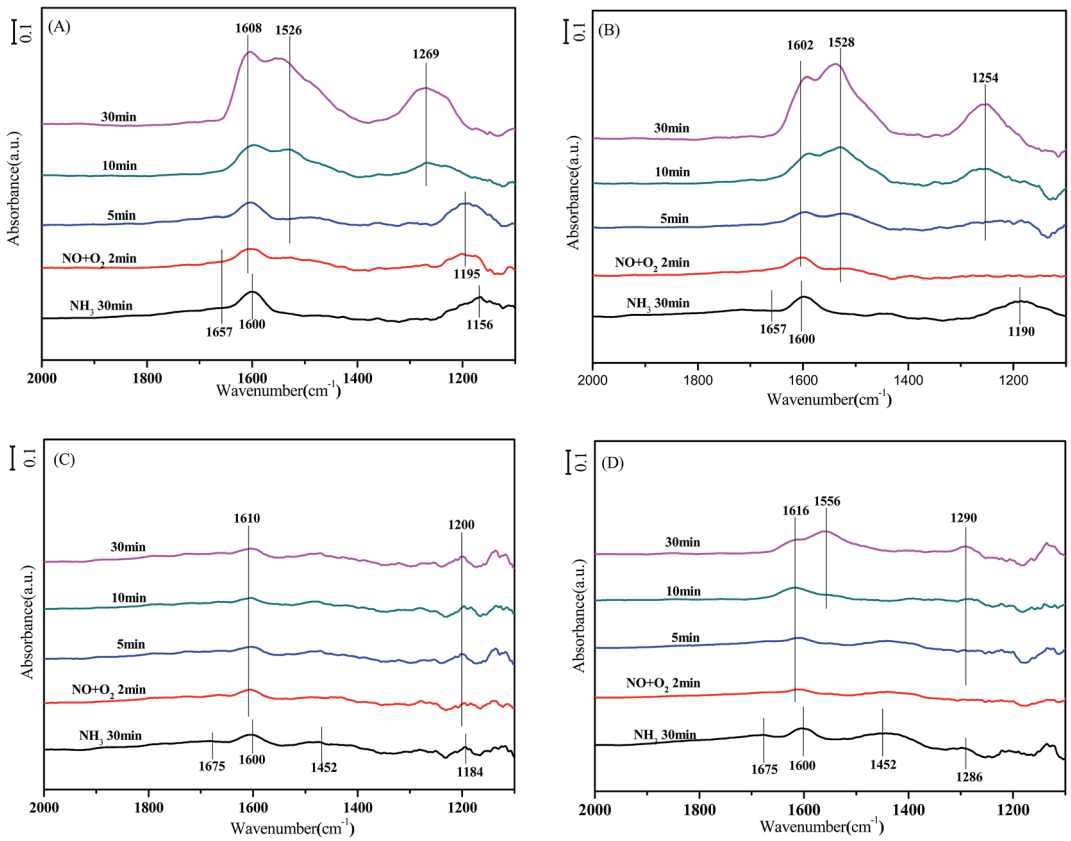

Fig. 10 DRIFT spectra of the reaction between NO + O_2 and preadsorbed NH_3 species over (A) Mn–Ti; (B) Mn–Mo–Ti; (C) Mn–Ti–P and (D) Mn–Mo–Ti–P at 200 °C.

pointed that the presence of more Mn^{4+} could generate more empty orbitals, which is helpful to the formation of Lewis acid sites for NH_3 adsorption. So the results of DRIFT study are also in accordance with that of XPS study. In addition, the band intensities decrease with increasing temperature, indicating the desorption of adsorbed NH_3 species from catalyst surface. It could be observed that all the bands due to Brønsted acid sites in the spectra of Mn–Ti catalyst nearly disappear at about 250 °C, while the band at 1190 cm^{-1} in the spectra of Mn–Mo–Ti catalyst is still present. Therefore, the NH_3 species adsorbed on Lewis acid sites are more thermally stable than that adsorbed on Brønsted acid sites, as indicated by Chen *et al.*[82] The DRIFT spectra of NH_3 adsorption over the two poisoned catalyst samples are shown in Fig. 8(C) and (D) respectively, it can be seen that the adsorption of NH_3 species over the two poisoned catalyst samples are greatly suppressed by the presence of P, however, the band intensities in the spectra of Mn–Mo–Ti–P are still higher than that in the spectra of Mn–Ti–P catalyst.

3.8.2 NO + O_2 co-adsorption. The DRIFT spectra of NO + O_2 co-adsorption over Mn–Ti and Mn–Mo–Ti at different catalyst samples are shown in Fig. 9. For the spectra of Mn–Ti catalyst, four bands could be found, which might be assigned to adsorbed NO_2 species (1610 cm^{-1}), bidentate nitrate (1557 and 1236 cm^{-1}) and monodentate nitrate (1285 cm^{-1}).[1,76,82–84] For Mn–Mo–Ti catalyst, the DRIFT spectra is very similar with that of Mn/TiO_2 catalyst, and the two different bands at 1271 and 1225 cm^{-1} could be attributed to monodentate nitrate and bridged nitrate respectively.[85,86] And the intensities of the bands in Fig. 9(A) is very close to that of the bands in Fig. 9(B). Moreover, the DRIFT spectra of NO + O_2 co-adsorption over Mn–Ti–P and Mn–Mo–Ti–P are presented in Fig. 9(C) and (D) respectively. Compared with the DRIFT spectra of the two fresh samples, an obvious band intensity drop could be found in the DRIFT spectra of the two poisoned samples, thus the loading of P also inhibit the adsorption of NO_x on Mn-based SCR catalyst, as reported in our previous study.[50]

3.8.3 Reaction between NO_x and preadsorbed NH_3 species. Prior to the adsorption of NO_x, the catalyst sample was pretreated by 600 ppm NH_3/N_2 at 200 °C for 30 min. After purging with N_2 for 15 min, 600 ppm NO + 5% O_2/Ar was introduced to the DRIFT cell and the DRIFT spectra were recorded with reaction time. As shown in Fig. 10(A), several bands of adsorbed NH_3 species (1657, 1600 and 1156 cm^{-1}) appeared in the DRIFT spectra of Mn–Ti catalyst after the pretreatment with NH_3. After the introduction of NO + O_2, all these bands quickly vanished in 2 min, indicating the high reactivity of the adsorbed NH_3 species. Thus all the adsorbed NH_3 species could take part in the NH_3-SCR reaction over Mn–Ti catalyst, meanwhile, several bands of adsorbed NO_x species formed and grew with time. For Mn–Mo–Ti catalyst, the DRIFT spectra are similar with that of

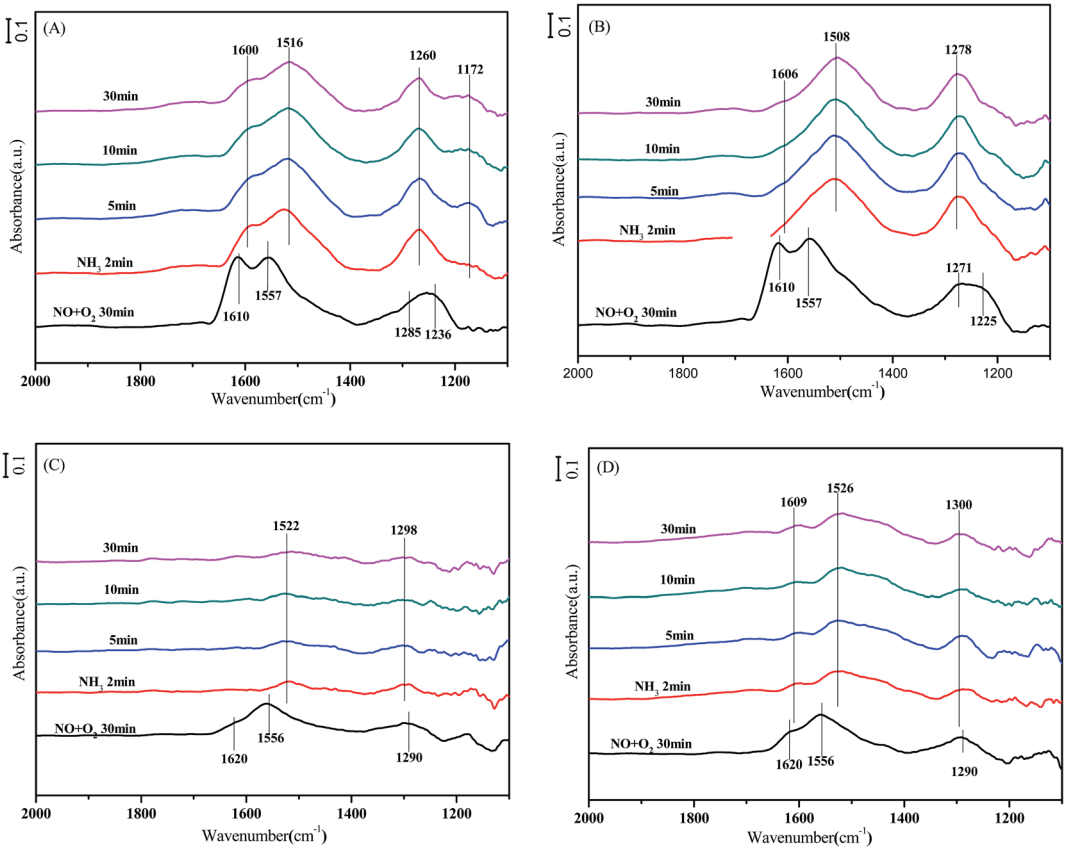

Fig. 11 DRIFT spectra of the reaction between NH_3 and preadsorbed NO_x species over (A) Mn–Ti; (B) Mn–Mo–Ti; (C) Mn–Ti–P and (D) Mn–Mo–Ti–P at 200 °C.

Mn/TiO_2 catalyst, all the adsorbed NH_3 species exhibited high reactivity in the NH_3-SCR reaction over it. Thus the Eley–Rideal (E–R) mechanism is suitable to the NH_3-SCR reactions over the two fresh catalyst samples.[62] Furthermore, the DRIFT spectra of the reaction between NO + O_2 and preadsorbed NH_3 species over the two poisoned catalyst samples are shown in Fig. 10(C) and (D). Similar conclusion could be drawn from the results illustrated in Fig. 10(C) and (D), it seems that the addition of P only inhibit the adsorption of NH_3 species over the two fresh catalyst samples, but the reactivity of adsorbed NH_3 species over Mn–Ti–P and Mn–Mo–Ti–P are still as high as that over the two fresh catalyst samples.

3.8.4 Reaction between NH_3 and preadsorbed NO_x species. In this experiment, the catalyst sample was pre-exposed to 600 ppm NO + 5% O_2/N_2 at 200 °C for 30 min. After purging with N_2 for 15 min, 600 ppm NH_3/Ar was introduced to the cell and the DRIFT spectra were recorded with the variation of time, as illustrated in Fig. 11. As can be seen from Fig. 11(A) and (B), the spectra of Mn–Ti and Mn–Mo–Ti are basically similar. Several bands of adsorbed NO_x species could be detected in the spectra of the two fresh catalyst samples after the exposure to NO + O_2. And all the bands of adsorbed NO_x species vanished after the introduction of NH_3 in about 2 min. Therefore, all the adsorbed NO_x species are active in the NH_3-SCR reactions over Mn–Ti and Mn–Mo–Ti. The results indicate that the NH_3-SCR reactions over the two fresh catalyst samples are also under the control of Langmuir–Hinshelwood (L–H) mechanism,[63] in which the adsorbed NO_x species react with the adsorbed NH_3 species to form N_2 and H_2O. For the two poisoned catalyst samples, the DRIFT spectra under the sane conditions are shown in Fig. 11(C) and (D). Similarly, the reactivities of adsorbed NO_x species over the two poisoned catalyst samples have not been weakened by the addition of P, except that the decreased adsorption amount of them. In summary, the addition of Mo on Mn–Ti catalyst does not change the NH_3-SCR reaction mechanism over it. The NH_3-SCR reactions over Mn–Ti and Mn–Mo–Ti are governed by the combination of E–R and L–H mechanisms, which is also reported by Meng *et al.*[81] and Yang *et al.*[87] for Mn-based SCR catalysts.

3.9 Reaction mechanism

As can be seen from Fig. 1(A), the NH_3-SCR reaction over the two poisoned catalyst samples is greatly dependent on the reaction temperature, and the deactivation effect is more serious at lower temperature range. In order to further understand the promotion mechanism of Mo modification on the P resistance of Mn–Ti catalyst, the effect of reaction temperature on the mechanism of the NH_3-SCR reactions over the four catalyst samples should be investigated.

Based on the method proposed by Yang *et al.*,[87] the mechanism of NH_3-SCR reaction over a catalyst could be determined by varying the NO inlet concentration. In this process, the inlet concentrations of NO and NH_3 remain the same to ensure full

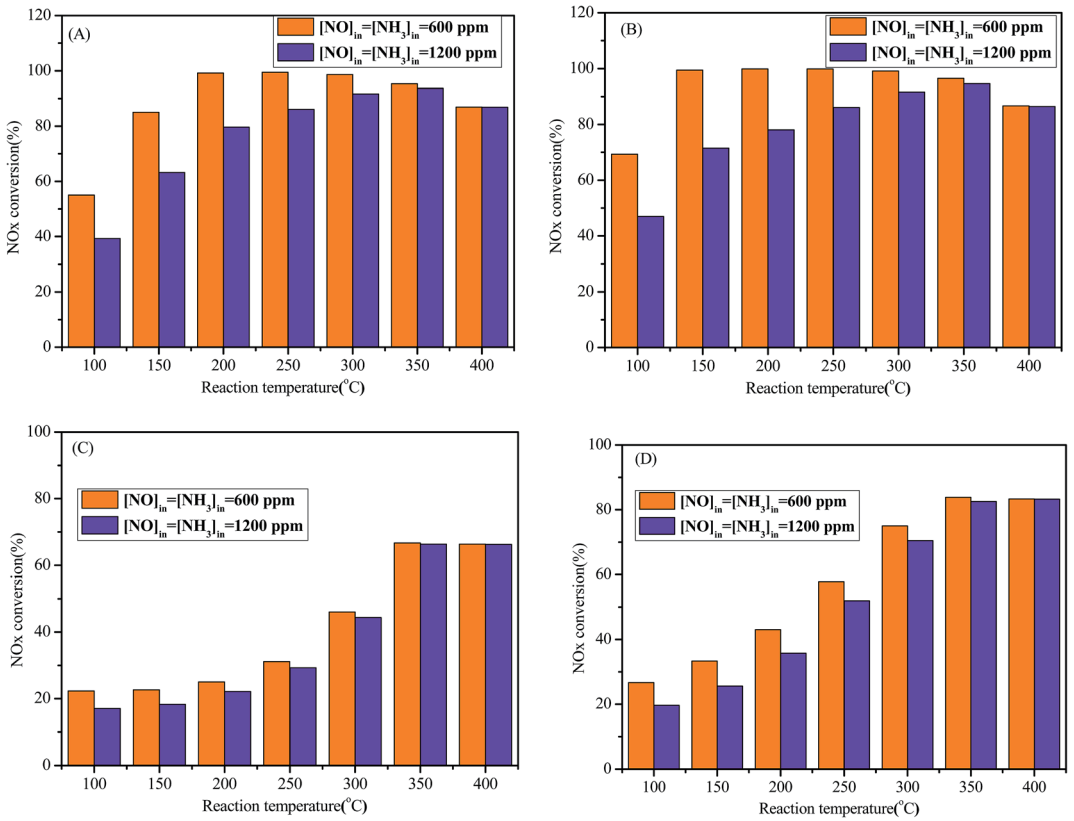

Fig. 12 Influence of NO inlet concentration on NO_x conversion over (A) Mn–Ti; (B) Mn–Mo–Ti; (C) Mn–Ti–P and (D) Mn–Mo–Ti–P at different temperature reaction conditions: [NO] = [NH_3] = 600 ppm or [NO] = [NH_3] = 1200 ppm, [O_2] = 5%, balance Ar, GHSV = 108 000 h^{-1}.

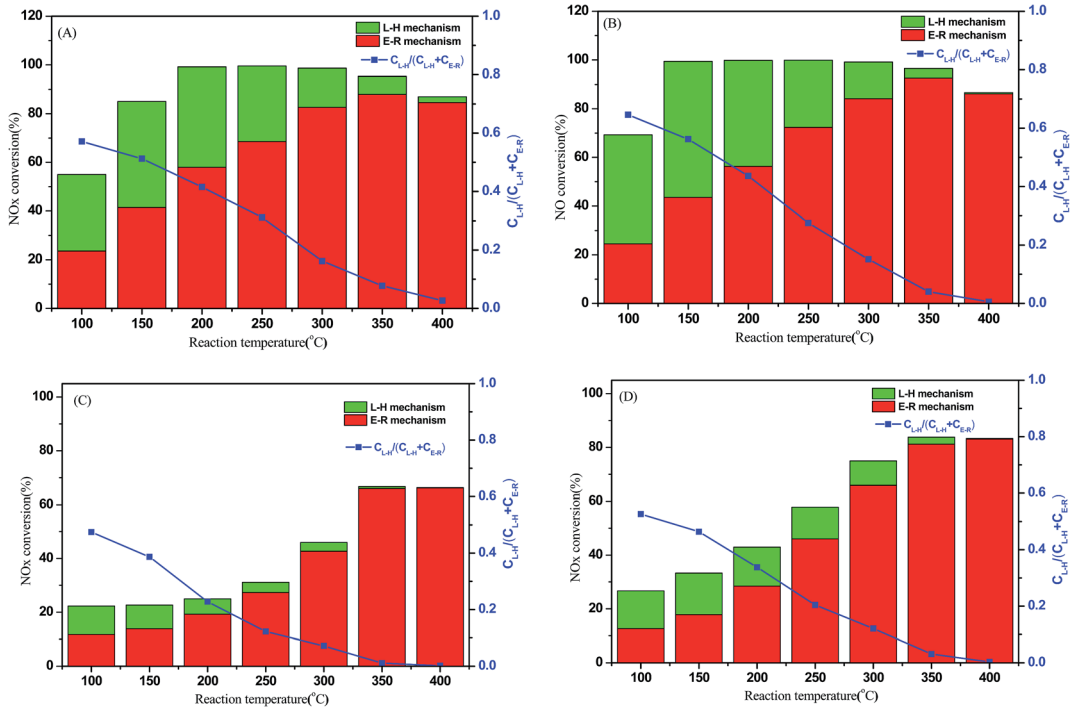

Fig. 13 Contributions of E–R and L–H mechanisms to the NH_3-SCR reactions over: (A) Mn–Ti; (B) Mn–Mo–Ti; (C) Mn–Ti–P and (D) Mn–Mo–Ti–P at different temperature reaction conditions: [NO] = [NH_3] = 600 ppm, [O_2] = 5%, balance Ar, GHSV = 108 000 h^{-1}.

reaction. If the SCR reaction over a catalyst was mainly controlled by E–R mechanism, the NO_x conversion should not decrease with the increase of NO inlet concentration from 600 ppm to 1200 ppm; in the other aspect, the NO_x conversion should halve under the same conditions change for a NH_3-SCR reaction mainly controlled by L–H mechanism. From Fig. 12, it can be observed that the NO_x conversions over Mn–Ti and Mn–Mo–Ti decrease after the NO inlet concentration increases from 600 ppm to 1200 ppm, but the values don't halve. The results further proven the coexistence of E–R and L–H mechanisms in the NH_3-SCR reactions over Mn–Ti and Mn–Mo–Ti, as mentioned above. For the two poisoned catalysts, similar conclusions could be drawn from the results shown in Fig. 12(C) and (D).

Moreover, the contributions of E–R and L–H mechanisms to the NH_3-SCR reactions over Mn–Ti and Mn–Mo–Ti could be obtained, as exhibited in Fig. 13. And the ratio of $C_{L-H}/(C_{L-H} + C_{E-R})$ represents the contribution of L–H mechanism to NH_3-SCR reaction, where C_{L-H} and C_{E-R} are the SCR reaction rates through L–H and E–R pathways respectively (normalized by BET surface area). From Fig. 13, it can be seen that the NH_3-SCR reactions over Mn–Ti and Mn–Mo–Ti are mainly governed by L–H mechanism (≤200 °C) and E–R mechanism (>200 °C) respectively. The promoted NH_3 adsorption over Mn–Mo–Ti catalyst could be favorable to the NH_3-SCR reaction over it through both L–H and E–R mechanisms, thereafter, enhancing its P resistance. From Fig. 13(C) and (D), it is clear that E–R mechanism is the main pathway for the NH_3-SCR reactions over the two poisoned catalyst samples. It is well recognized that the adsorption of NH_3 species is the key step for the NH_3-SCR reaction through E–R pathway; therefore, the presence of more adsorbed NH_3 species Mn–Mo–Ti–P could facilitate the SCR reaction over it. As a result, Mn–Mo–Ti–P catalyst shows better SCR performance than Mn–Ti–P catalyst.

4. Conclusions

In this study, it was found that the modification of Mn–Ti catalyst could enhance its resistance to P species in NH_3-SCR reaction. The characterization results indicated that the doping of Mo on Mn–Ti catalyst could increase the specific area and restrain the crystallization of TiO_2, and enhance the reducibility and NH_3 adsorption capacity, along with the formation of more surface chemisorbed oxygen species. All these features are helpful to promote the SCR performance of Mn–Ti catalyst. The results of *in situ* DRIFT study revealed that the addition of Mo on Mn–Ti catalyst did not change the mechanism of NH_3-SCR reaction over it, which is a combination of E–R and L–H mechanisms. For the NH_3-SCR reactions over the two poisoned catalyst samples, it seemed that E–R mechanism was predominant. The introduction of Mo to Mn–Ti catalyst would provide more Lewis acid sites for NH_3 adsorption, and the adsorbed NH_3 species are all active in the NH_3-SCR reactions over the two fresh catalyst samples.

Acknowledgements

This work was supported by the Natural Science Foundation of China (21546014) and the Natural Science Foundation of Shanghai, China (14ZR1417800).

Notes and references

1 Z. Lian, F. Liu and H. He, *Ind. Eng. Chem. Res.*, 2014, **53**, 19506–19511.
2 S. Deng, T. Meng, B. Xu, F. Gao, Y. Ding, L. Yu and Y. Fan, *ACS Catal.*, 2016, **6**, 5807–5815.
3 N. Yang, R. Guo, Y. Tian, W. Pan, Q. Chen, Q. Wang, C. Lu and S. Wang, *Fuel*, 2016, **179**, 305–311.
4 T. Boningari and P. G. Smirniotis, *Curr. Opin. Chem. Eng.*, 2016, **13**, 133–141.
5 J. Li, H. Chang, L. Ma, J. M. Hao and Y. T. Yang, *Catal. Today*, 2011, **175**, 147–156.
6 C. Liu, J. Shi, C. Gao and C. Niu, *Appl. Catal., A*, 2016, **522**, 54–69.
7 D. K. Pappas, T. Boningari, P. Boolchand and P. G. Smirniotis, *J. Catal.*, 2016, **334**, 1–13.
8 E. Park, M. Kim, H. Jung, S. Chin and J. Jurng, *ACS Catal.*, 2013, **3**, 1518–1525.
9 S. S. R. Putluru, L. Schill, A. D. Jensen, B. Siret, F. Tabaries and R. Fehrmann, *Appl. Catal., B*, 2015, **165**, 628–635.
10 B. Thirupathi and P. G. Smirniotis, *J. Catal.*, 2012, **288**, 74–83.
11 J. P. Dunn, P. R. Koppula, H. G. Koppula and I. E. Wachs, *Appl. Catal., B*, 1998, **19**, 103–117.
12 Y. Li, Y. Wan, Y. Li, S. Zhan, Q. Guan and Y. Tian, *ACS Appl. Mater. Interfaces*, 2016, **8**, 5224–5233.
13 Z. Chen, F. Wang, H. Li, Q. Yang, L. Wang and X. Li, *Ind. Eng. Chem. Res.*, 2012, **51**, 202–212.
14 P. Wang, Q. Wang, X. Ma, R. Guo and W. Pan, *Catal. Commun.*, 2015, **71**, 84–87.
15 F. Castellino, A. D. Jensen, J. E. Johnsson and R. Fehrmann, *Appl. Catal., B*, 2009, **86**, 206–215.
16 S. S. R. Putluru, A. D. Jensen, A. Riisager and R. Fehrmann, *Catal. Sci. Technol.*, 2011, **1**, 631–637.
17 F. Tang, B. Xu, H. Shi, J. Qiu and Y. Fan, *Appl. Catal., B*, 2010, **94**, 71–76.
18 A. Larsson, J. Einvall, A. Andersson and M. Sanati, *Energy Fuels*, 2006, **20**, 1398–1405.
19 Y. Jiang, X. Gao, Y. Zhang, W. Wu, H. Song, Z. Luo and K. Cen, *J. Hazard. Mater.*, 2014, **274**, 270–278.
20 F. Castellino, S. B. Rasmussen, A. D. Jensen, J. E. Johnsson and R. Fehrmann, *Appl. Catal., B*, 2008, **83**, 110–122.
21 M. Klimczak, P. Kern, T. Heinzelmann, M. Lucas and P. Claus, *Appl. Catal., B*, 2010, **95**, 39–47.
22 Y. Liu, Z. Liu, B. Mnichowicz, A. V. Harinath, H. Li and B. Bahrami, *Chem. Eng. J.*, 2016, **287**, 680–690.
23 C. Fang, D. Zhang, S. Cai, L. Zhang, L. Huang, H. Li, P. Maitarad, L. Shi, R. Gao and J. Zhang, *Nanoscale*, 2013, **5**, 9199–9207.
24 M. Wallin, S. Forser, P. Thormählen and M. Skoglundh, *Ind. Eng. Chem. Res.*, 2004, **43**, 7723–7731.
25 G. S. Qi and R. T. Yang, *Appl. Catal., B*, 2003, **44**, 217–225.
26 W. Li, R. T. Guo, S. X. Wang, W. G. Pan, Q. L. Chen, M. Y. Li, P. Sun and S. M. Liu, *RSC Adv.*, 2016, **6**, 82707–82715.
27 P. G. Smirniotis, D. A. Pena and B. S. Uphade, *Angew. Chem., Int. Ed.*, 2011, **40**, 2479–2482.
28 P. R. Ettireddy, A. Kotrba, T. Boningari and P. G. Smirniotis, *SAE Tech. Pap. Ser.*, 2015, 2015-01-1026.
29 P. R. Ettireddy, N. Ettireddy, T. Boningari, R. Pardemann and P. G. Smirniotis, *J. Catal.*, 2012, **292**, 53–63.
30 P. R. Ettireddy, N. Ettireddy, S. Mamedov, P. Boolchand and P. G. Smirniotis, *Appl. Catal., B*, 2007, **76**, 123–134.
31 B. Thirupathi and P. G. Smirniotis, *Appl. Catal., B*, 2011, **110**, 195–206.
32 S. Andreoli, F. A. Deorsola, C. Galletti and R. Pirone, *Chem. Eng. J.*, 2015, **278**, 174–182.
33 K. S. Kijlstra, D. S. Brands, H. I. Smit, E. K. Poels and A. Bliek, *J. Catal.*, 1997, **171**, 219–230.
34 G. Qi and R. T. Yang, *J. Catal.*, 2003, **217**, 434–441.
35 G. Marbán, T. Valdés-Solís and A. B. Fuertes, *Phys. Chem. Chem. Phys.*, 2004, **6**, 453–464.
36 X. N. Lu, C. Y. Song, S. H. Jia, Z. S. Tong, X. L. Tang and Y. X. Teng, *Chem. Eng. J.*, 2015, **260**, 776–784.
37 B. Greenhalgh, M. Fee, A. Dobri, J. Moir, R. Burich, J. P. Charland and M. Stanciulescu, *J. Mol. Catal. A: Chem.*, 2010, **333**, 121–127.
38 Y. J. Kim, H. J. Kwon, I. Nam, J. W. Choung, J. K. Kil, H. Kim, M. Cha and G. K. Yeo, *Catal. Today*, 2010, **151**, 244–250.
39 D. Fang, J. L. Xie, H. Hu, Z. Zhang, F. He, Y. Zheng and Q. Zhang, *Fuel Process. Technol.*, 2015, **134**, 465–472.
40 Y. Liu, T. Gu, Y. Wang, X. Weng and Z. Wu, *Catal. Commun.*, 2012, **18**, 106–109.
41 L. Zhang, S. Cui, H. Guo, X. Ma and X. Luo, *Appl. Surf. Sci.*, 2015, **355**, 1116–1122.
42 R. Guo, Q. Wang, W. Pan, Q. Chen, H. Ding, X. Yin, N. Yang, C. Lu, S. Wang and Y. Yuan, *J. Mol. Catal. A: Chem.*, 2015, **407**, 1–7.
43 Y. Peng, J. H. Li, W. Z. Si, X. Li, W. B. Shi, J. M. Luo, J. Fu, J. Crittenden and J. Hao, *Chem. Eng. J.*, 2015, **269**, 44–50.
44 X. P. Zhang, Y. Z. Cui, Z. F. Li, X. R. Zhou and G. H. He, *Chem. Eng. Technol.*, 2016, **39**, 874–882.
45 W. Li, R. T. Guo, S. X. Wang, W. G. Pan, Q. L. Chen, M. Y. Li, P. Sun and S. M. Liu, *Fuel Process. Technol.*, 2016, **154**, 235–242.
46 L. M. Ottosen, G. M. Kirkelund and P. E. Jensen, *Chemosphere*, 2013, **91**, 963–969.
47 M. Cyr, M. Coutand and P. Clastres, *Cem. Concr. Res.*, 2007, **37**, 1278–1289.
48 S. Andonova, E. Vovk, J. Sjöblom, E. Ozensoy and L. Olsson, *Appl. Catal., B*, 2014, **147**, 251–263.
49 S. Shwan, J. Jansson, L. Olsson and M. Skoglundh, *Appl. Catal., B*, 2014, **147**, 111–123.
50 N. Yang, R. Guo, Q. Wang, W. Pan, Q. Chen, C. Lu and S. Wang, *RSC Adv.*, 2016, **6**, 11226–11232.
51 X. Li, X. Li, J. Li and J. Hao, *J. Hazard. Mater.*, 2016, **318**, 615–622.
52 F. Wang, H. Dai, J. Deng, G. Bai, K. Ji and Y. Liu, *Environ. Sci. Technol.*, 2012, **46**, 4034–4041.
53 R. Guo, Q. Wang, W. Pan, W. Zhen, Q. Chen, H. Ding, N. Yang and C. Lu, *Appl. Surf. Sci.*, 2014, **317**, 111–116.
54 F. D. Liu, H. He, Y. Ding and C. B. Zhang, *Appl. Catal., B*, 2009, **93**, 194–204.
55 M. Kang, E. D. Park, J. M. Kim and J. E. Yie, *Appl. Catal., A*, 2007, **327**, 261–269.

56 L. Zhang, D. Zhang, J. Zhang, S. Cai, C. Fang, L. Huang, H. Li, R. Gao and L. Shi, *Nanoscale*, 2013, **5**, 9821–9829.
57 X. Huang, Z. Ma, W. Lin, F. Liu and H. Yang, *Catal. Commun.*, 2017, **91**, 53–56.
58 L. Arnarson, H. Falsig, S. B. Rasmussen, J. V. Lauritsen and P. G. Moses, *J. Catal.*, 2017, **346**, 188–197.
59 X. Wang, Z. Lan, Y. Liu, Y. Luo, J. Chen, L. Jiang and Y. Wang, *Chem. Commun.*, 2017, **53**, 967–970.
60 F. Larachi, J. Pierre, A. Adnot and A. Bernis, *Appl. Surf. Sci.*, 2002, **195**, 236–250.
61 H. Wang, X. Chen, S. Gao, Z. Wu, Y. Liu and X. Weng, *Catal. Sci. Technol.*, 2013, **3**, 715–722.
62 Y. Chen, J. P. Wang, Z. Yan, L. L. Liu, Z. T. Zhang and X. D. Wang, *Catal. Sci. Technol.*, 2015, **5**, 2251–2259.
63 R. Guo, Y. Zhou, W. Pan, J. Hong, W. Zhen, Q. Jin, C. Ding and S. Guo, *J. Ind. Eng. Chem.*, 2013, **19**, 2022–2025.
64 Q. Zhang, C. Qiu, H. Xu, T. Lin, Z. Lin, M. Gong and Y. Chen, *Catal. Today*, 2011, **175**, 171–176.
65 P. Maitarad, D. S. Zhang, R. H. Gao, L. Y. Shi, H. R. Li, L. Huang, T. Rungrotmongkol and J. P. Zhang, *J. Phys. Chem. C*, 2013, **117**, 9999–10006.
66 X. Wang, Y. Y. Zheng, Z. Xu, X. L. Wang and X. P. Chen, *RSC Adv.*, 2013, **3**, 11539–11542.
67 N. Y. Topsøe, *Science*, 1994, **265**, 1217–1219.
68 X. Du, X. Gao, R. Qu, P. Ji, Z. Luo and K. Cen, *ChemCatChem*, 2012, **4**, 2075–2081.
69 B. Guan, H. Lin, L. Zhu, B. Tian and Z. Huang, *Chem. Eng. J.*, 2012, **181–182**, 307–322.
70 Q. Chen, R. Guo, Q. Wang, W. Pan, W. Wang, N. Yang, C. Lu and S. Wang, *Fuel*, 2016, **181**, 852–858.
71 R. P. Vélez, I. Ellmers, H. Huang, U. Bentrup, W. Schünemann, W. Grünert and A. Brückner, *J. Catal.*, 2014, **316**, 103–111.
72 F. Gao, M. Kollár, R. K. Kukkadapu, N. M. Washton, Y. Wang, J. Szanyi and C. F. H. Peden, *Appl. Catal., B*, 2015, **164**, 407–419.
73 R. Guo, Q. Chen, H. Ding, Q. Wang, W. Pan, N. Yang and C. Lu, *Catal. Commun.*, 2015, **69**, 165–169.
74 Y. Peng, J. Li, X. Huang, X. Li, W. Su, D. Wang and J. Hao, *Environ. Sci. Technol.*, 2014, **48**, 4515–4520.
75 S. Wang, R. Guo, W. Pan, M. Li, P. Sun, S. Liu, S. Liu, X. Sun and J. Liu, *Phys. Chem. Chem. Phys.*, 2017, **19**, 5333–5342.
76 Z. Wu, B. Jiang, Y. Liu, H. Wang and R. Jin, *Environ. Sci. Technol.*, 2007, **41**, 5812–5817.
77 J. Li, J. Chen, R. Ke, C. Luo and J. Hao, *Catal. Commun.*, 2007, **8**, 1896–1900.
78 D. Nicosia, I. Czekaj and O. Kröcher, *Appl. Catal., B*, 2008, **77**, 228–236.
79 P. Sun, R. Guo, S. Liu, S. Wang, W. Pan and M. Li, *Appl. Catal., A*, 2017, **531**, 129–138.
80 Y. Liu, T. T. Gu, X. L. Weng, Y. Wang, Z. B. Wu and H. Q. Wang, *J. Phys. Chem. C*, 2012, **116**, 16582–16592.
81 D. Meng, W. Zhan, Y. Guo, Y. Guo, L. Wang and G. Lu, *ACS Catal.*, 2015, **5**, 5973–5983.
82 L. Chen, J. Li and M. Ge, *Environ. Sci. Technol.*, 2010, **44**, 9590–9596.
83 Z. Liu, J. Zhu, J. Li, L. Ma and S. I. Woo, *ACS Appl. Mater. Interfaces*, 2014, **6**, 14500–14508.
84 M. Adamowska, A. Krztoń, M. Najbar, P. D. Costa and G. Djéga-Mariadassou, *Catal. Today*, 2008, **137**, 288–291.
85 H. Hu, S. X. Cai, H. R. Li, L. Huang, L. Y. Shi and D. S. Zhang, *J. Phys. Chem. C*, 2015, **119**, 22924–22933.
86 N. Yang, R. Guo, W. Pan, Q. Chen, Q. Wang, C. Lu and S. Wang, *Appl. Surf. Sci.*, 2016, **378**, 513–518.
87 S. Yang, C. Wang, J. Li, N. Yan, L. Ma and H. Chang, *Appl. Catal., B*, 2011, **110**, 71–80.